Manipulating Surface-Related Ferromagnetism in Modulation-Doped Topological Insulators

Xufeng Kou,[†,∥] Liang He,*[†,∥] Murong Lang,[†,∥] Yabin Fan,[†] Kin Wong,[†] Ying Jiang,[‡] Tianxiao Nie,[†] Wanjun Jiang,[†] Pramey Upadhyaya,[†] Zhikun Xing,[†] Yong Wang,[‡] Faxian Xiu,[§] Robert N. Schwartz,[†] and Kang L. Wang*[†]

[†]Device Research Laboratory, Department of Electrical Engineering, University of California, Los Angeles, California 90095, United States

[‡]Center for Electron Microscopy and State Key Laboratory of Silicon Materials, Department of Materials Science and Engineering, Zhejiang University, Hangzhou 310027, China

[§]Department of Electrical and Computer Engineering, Iowa State University, Ames, Iowa 50011, United States

Ⓢ Supporting Information

ABSTRACT: A new class of devices based on topological insulators (TI) can be achieved by the direct engineering of the time-reversal-symmetry (TRS) protected surface states. In the meantime, a variety of interesting phenomena are also expected when additional ferromagnetism is introduced to the original topological order. In this Letter, we report the magnetic responses from the magnetically modulation-doped $(Bi_zSb_{1-z})_2Te_3/Cr_x(Bi_ySb_{1-y})_2Te_3$ bilayer films. By electrically tuning the Fermi level across the Dirac point, we show that the top TI surface carriers can effectively mediate the magnetic impurities and generate robust ferromagnetic order. More importantly, such surface magneto-electric effects can be either enhanced or suppressed, depending on the magnetic interaction range inside the TI heterostructures. The manipulation of surface-related ferromagnetism realized in our modulation-doped TI device is important for the realization of TRS-breaking topological physics, and it may also lead to new applications of TI-based multifunctional heterostructures.

KEYWORDS: Topological insulator, modulation-doped growth, TI heterostructures, surface-related magnetism
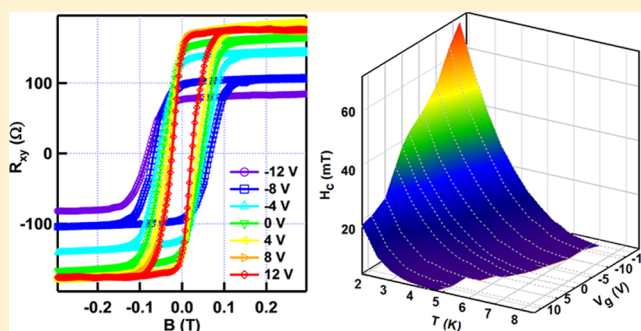
When the spin−orbit coupling is strong enough to invert the conduction and valence bands in the material, it creates a new state of matter, known as the time-reversal-invariant Z_2 topological insulators (TIs).[1−7] This unique material system offers topologically protected surface states which can be utilized to realize dissipationless spin-dependent transport.[8−11] Alternatively, it is also important to break the time-reversal-symmetry (TRS) of the nontrivial TI material by combining external perpendicular ferromagnetic coupling.[12−15] In this TRS-breaking regime, the opened surface gap will give rise to a variety of novel physical phenomena such as the quantum anomalous Hall effect,[14−18] single chiral mode conduction,[19−22] and axion electrodynamics.[23−27]

Introducing magnetic ions into the TI materials has been proven to be an effective way to generate robust magnetism and open a gap of the surface states.[13,28−34] Theoretically, it has been proposed that in magnetically doped TI systems, ferromagnetic moments can be developed through two major mechanisms: the van Vleck mechanism from the large spin susceptibility of the valence electrons in TI materials,[15] and the Ruderman−Kittel−Kasuya−Yosida (RKKY) interaction between neighboring magnetic ions, which are mediated by

either the bulk itinerant carriers or the TI surface Dirac-fermions.[13,34] Recently, these two magnetic mechanisms were independently observed in uniformly doped $Mn−Bi_2Te_2Se_1$ and $Cr-(BiSb)_2Te_3$ systems, respectively.[35,36] It is noted that since the magnetic dopants distribute homogeneously inside such uniform magnetic TI thin films, it is difficult to quantify the surface-related magnetism from the total signals (which contain the bulk, top, and bottom surfaces). Moreover, the interplay between the surface and bulk magnetizations and the controllability of each contribution are still debated.

In the present work, instead of studying the uniform doping case, we prepare the $(Bi_zSb_{1-z})_2Te_3/Cr_x(Bi_ySb_{1-y})_2Te_3$ bilayer films using the modulation-doped growth method. By controlling the separation between the top topological surface and the bottom Cr-doped magnetic TI layer, we identify the presence of surface-related ferromagnetism from magneto-optical Kerr measurements. Furthermore, with effective gate modulation the surface-mediated magnetization of the TI/Cr-
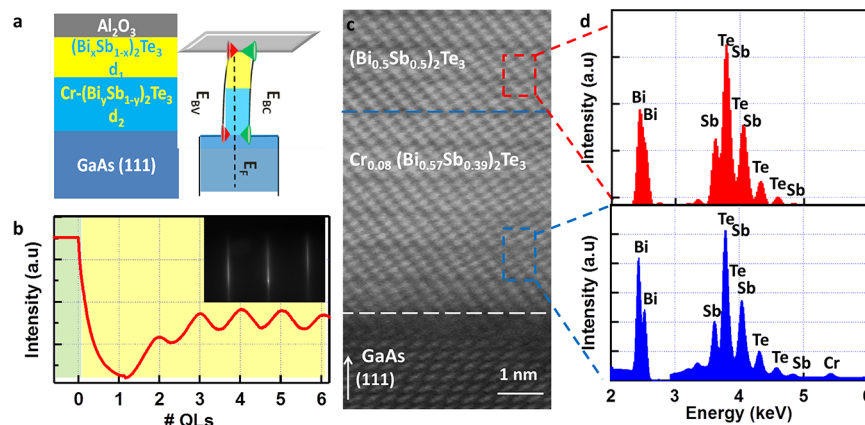
Figure 1. TI/modulation-doped $(Bi_xSb_{1-x})_2Te_3$/Cr-$(Bi_ySb_{1-y})_2Te_3$ bilayer structure and thin film characterizations. (a) Schematic layout and energy band diagram for the bilayer device consisting of one $(Bi_xSb_{1-x})_2Te_3$ layer on top of another Cr-$(Bi_ySb_{1-y})_2Te_3$ layer. The composition ratio of x and y is carefully chosen so that the two channels have similar low conductivities and bulk carrier densities. (b) RHEED oscillations used to monitor the growth conditions and control the thin film thickness. Inset: A streaky RHEED pattern along the $[11\bar{2}0]$ direction of the as-grown surface that indicates a 2D growth mode. (c) High-resolution cross-section STEM image of the bilayer thin film DRL001. Typical quintuple-layered crystalline structure and sharp TI–GaAs interface can be clearly observed. No Cr segregations are detected, which indicates a uniform Cr distribution in the magnetic TI material matrix. (d) EDX spectrum of $(Bi_{0.5}Sb_{0.5})_2Te_3$ and $Cr_{0.08}(Bi_{0.57}Sb_{0.39})_2Te_3$ layers.
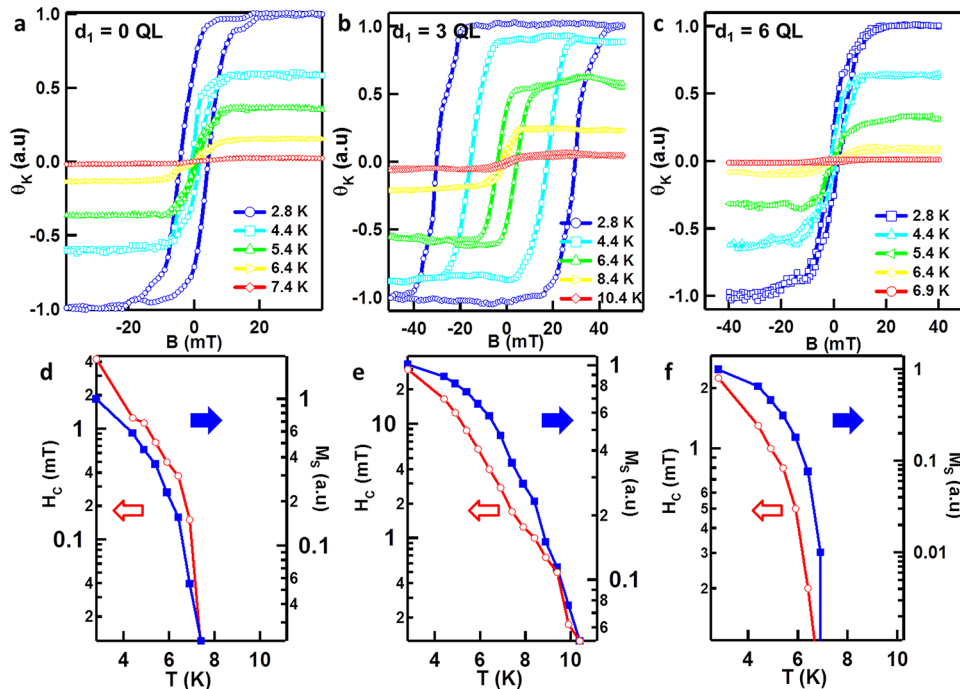

Figure 2. Temperature-dependent magnetization MOKE measurement. (a–c) Out-of-plane magnetizations (reflected in H_c) measured by a polar-mode MOKE setup. All of the modulation-doped samples have the same 6 QL $Cr_{0.16}(Bi_{0.54}Sb_{0.38})_2Te_3$ bottom layer with different top layer thicknesses (0 QL, 3 QL, and 6 QL). The largest magnetization is produced in the 3 QL TI/6 QL Cr-doped TI structure, which is consistent with transport measurements. (d–f) The extraction of the saturated magnetization M_s and coercivity field H_c from MOKE measurements.

doped TI heterostructures can be either amplified or suppressed, depending on the structure engineering. These electrically controllable topological surface phenomena may help us to broaden the understanding of magnetic topological insulators and expand the functionality of TI-based devices. It may also offer new opportunities to utilize the TI heterostructures (i.e., quantum wells and superlattices) in which interactions among different layers may result in even more exotic physics and applications.

To investigate the interaction between the magnetic impurities and surface Dirac carriers in magnetically doped

TIs, high quality Cr-doped $(Bi_xSb_{1-x})_2Te_3$ thin films are first prepared using molecular beam epitaxy (MBE). In contrast to the conventional uniform doping method, we use a modulation-doped method to produce the $(Bi_xSb_{1-x})_2Te_3$/Cr-$(Bi_ySb_{1-y})_2Te_3$ bilayer films by accurately controlling the Cr-dopant distribution profiles along the epitaxial growth direction.[37–39] The schematic layout and corresponding energy band diagram of such bilayer structures are shown in Figure 1a. During the sample growth, we use real-time reflection high-energy electron diffraction (RHEED) to in situ monitor the growth dynamics. Specifically, sharp streaky lines with the
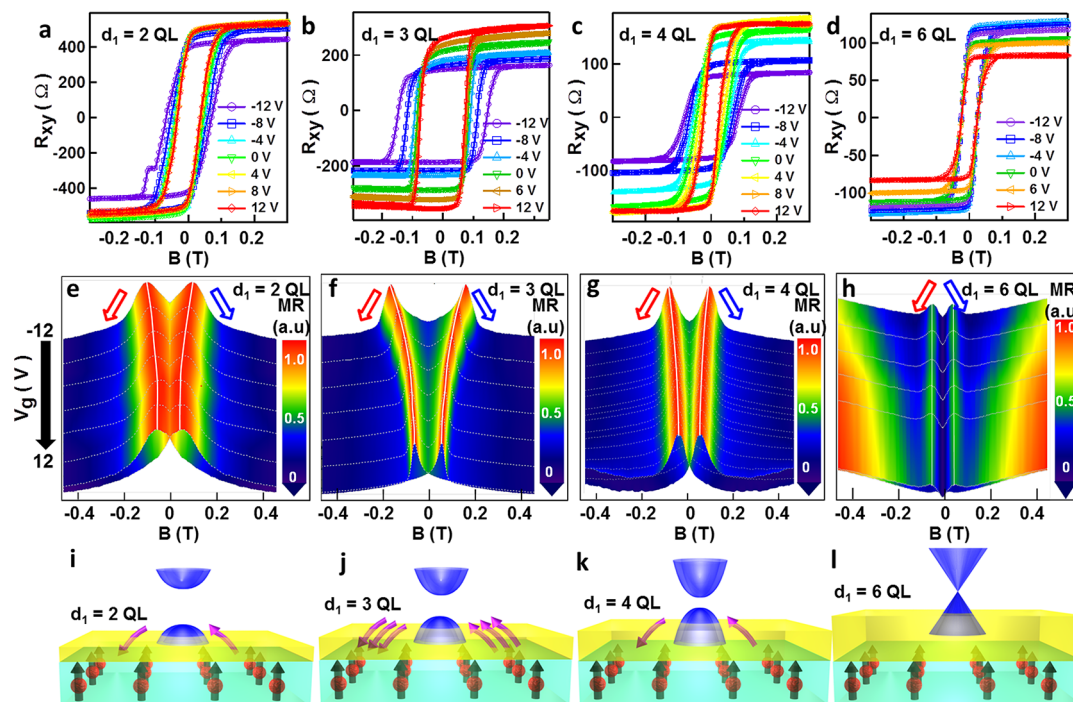
Figure 3. Surface-related magneto-electric effects in TI/Cr-doped TI bilayer structure. (a−d) Gate-dependent anomalous Hall effects on top-gated $(Bi_{0.5}Sb_{0.5})_2Te_3/Cr_{0.16}(Bi_{0.54}Sb_{0.38})_2Te_3$ bilayer structures. The bottom layer thickness is fixed as 6 QL, and the top layer thickness d_1 is selected from 2 QL, 3 QL, 4 QL, and 6 QL. The surface-related magneto-electric effect becomes most significant when $d_1 = 3$ QL, and disappears once $d_1 \geq 6$ QL. All of the data are collected at $T = 1.9$ K. (e−h) Electric-field-controlled longitudinal magneto-resistance MR on top-gated $(Bi_{0.5}Sb_{0.5})_2Te_3/Cr_{0.16}(Bi_{0.54}Sb_{0.38})_2Te_3$ bilayer heterostructures with different top layer thicknesses. Arrows indicate the sweeping directions of the magnetic field. Typical butterfly shapes can be observed, and the change of peak positions by gate bias is consistent with the change in the AHE curves. The WAL peak appears when $d_1 \geq 6$ QL and indicates the recovery of massless Dirac-fermions on the surface (Supporting Information Figure S8). (i−l) Schematic representations of the surface-related magneto-electric effects in TI/Cr-doped TI bilayer structures with different top layer thicknesses. Because the bulk magnetic moments are fixed inside the bottom layer, the mediation of RKKY exchange coupling by top surface states is determined by two competing factors, which include the separation of top surface states from chromium impurities, and the surface gap opening Δ_0.

bright specular spot persist the entire growth period, indicating a smooth 2D growth mode. In the meanwhile, by counting the RHEED oscillations displayed in Figures 1b, we are able to control the thickness of both the Cr-doped TI and pure TI layers with high accuracy (i.e., deviation < ±0.1 nm compared with the design value). Crystalline structure characterization is performed using high-resolution scanning transmission electron microscopy (HRSTEM). Figure 1c reveals the atomically sharp TI−GaAs interface and highly ordered tetradymite-type quintuple-layered (QL) structure (i.e., the lattice spacing of each QL ∼1 nm).[40] Such epitaxially ordered lattice configuration also confirms that there is no second phase segregation inside the TI thin film within the resolution of HRSTEM. In addition, the Bi/Sb composition ratio (x, y) and the Cr doping level are determined by an energy-dispersive X-ray (EDX) spectroscopy as shown in Figure 1d. In contrast to the lower figure, the absence of the Cr peak in the upper EDX spectrum provides strong evidence that the Cr atoms only distribute inside the bottom 6 QL $Cr_{0.08}(Bi_{0.57}Sb_{0.39})_2Te_3$ layer, while the top 3 QL layer is free of magnetic impurities (see details in the Supporting Information S2).

We have demonstrated that a moderate Cr doping of about 10% is sufficient enough to force the Dirac-conelike surface open the band gap (as discussed in Supporting Information Figure S3).[33] In this Letter, to ensure a solid comparison all of the modulation-doped TI bilayer samples have identical $Cr_{0.16}(Bi_{0.54}Sb_{0.38})_2Te_3$ bottom layers with the same film thickness of 6 QL, Bi/Sb ratio of 0.59/0.41, and the Cr doping

concentration of 8% (Supporting Information Figure S1c). As for the top undoped TI layers in these samples, we adjust the Bi/Sb ratio to be 0.5/0.5 so that the electrical conductivity is similar to that of the bottom Cr-doped TI layer (Supporting Information Figure S4). More importantly, the low densities obtained in both layers further ensure that the Fermi level E_F locates well-inside the bulk band gap, therefore minimizing the bulk conduction in the following magneto-transport measurements.[41−43]

The main objective of the following sections is to investigate the surface-related magnetism in the modulation-doped TI heterostructures. We first discuss the magneto-optical Kerr effect (MOKE) measurement as it offers a straightforward quantification of the magnetizations. Arising from the out-of-plane magnetic anisotropy in the Cr-doped TI systems, polar MOKE studies are carried out in three different samples as follows: Sample **A** (DRL003) has a 6 QL $Cr_{0.16}(Bi_{0.54}Sb_{0.38})_2Te_3$ with a uniform Cr-doping profile that serves as the control sample; Sample **B** (DRL005) and Sample **C** (DRL008) share the same 6 QL $Cr_{0.16}(Bi_{0.54}Sb_{0.38})_2Te_3$ designs in the bottom but differ in the top undoped $(Bi_{0.5}Sb_{0.5})_2Te_3$ layer thickness, namely 3 QL for Sample **B** and 6 QL for Sample **C**. Figure 2a−c shows the field-dependent MOKE results acquired at different temperatures. All of these three samples display nearly square-shaped ferromagnetic hysteresis loops at low temperatures, suggesting the robust ferromagnetic order with the easy axis perpendicular to the thin films. However, the magnitudes of their MOKE signals are
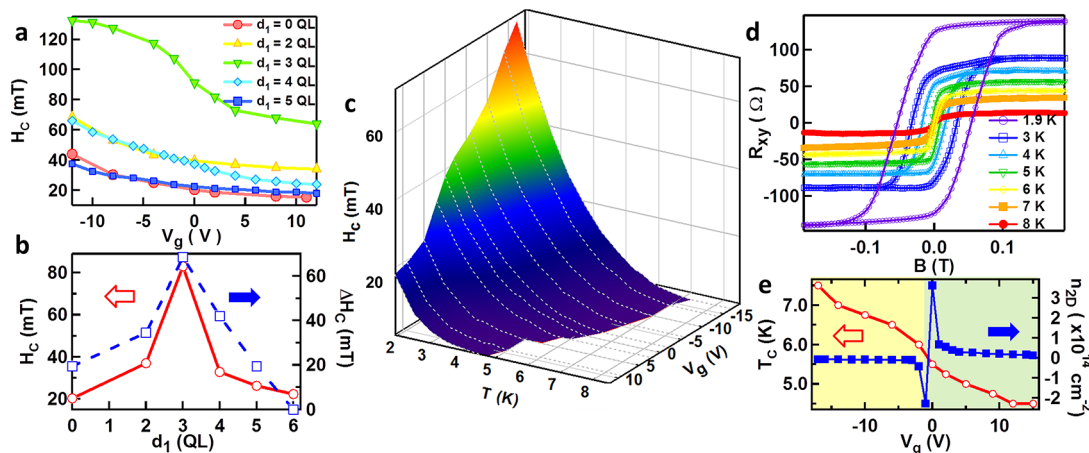
Figure 4. Enhancement of surface-mediated magneto-electric response and extraction of Curie temperature. (a) Gate-controlled coercivity field H_c of modulation-doped structures. The Cr-doped TI layer is fixed as 6 QL $Cr_{0.16}(Bi_{0.54}Sb_{0.38})_2Te_3$, whereas the thickness of the top undoped TI layer changes from 0 QL to 6 QL. All data are measured at 1.9 K. (b) Comparisons of the both the "neutral point" H_c and gate-controlled coercivity field change ΔH_c in modulation-doped samples with varying top surface thickness d_1. The "neutral point" is defined as the position where the surface Fermi levels are tuned close to the Dirac point. (c) Three-dimensional map of the coercivity field H_c under different gate biases and temperatures for the 4 QL $(Bi_{0.5}Sb_{0.5})_2Te_3$/6 QL $Cr_{0.16}(Bi_{0.54}Sb_{0.38})_2Te_3$ thin film. Curie temperature T_c is estimated from the temperature-dependent AHE effect where the hysteresis behavior disappears above T_c. (d) Temperature-dependent anomalous Hall effect under the applied gate voltage of -8 V. Many different data for various gate biases are used to construct panel c. (e) Electric-field dependent Curie temperature and 2D carrier density n_{2D} as functions of V_g. The overall Hall density n_{2D} exhibits a sign change at $V_g = 0$ V. T_c decreases monotonically when the majority carriers are changed from p-type to n-type, which is consistent with the hole-mediated RKKY mechanisms on the top surface.

dramatically different. On the one hand, when the top layer thickness d_1 is 3 QL, the coercivity field H_c at $T = 2.8$ K has enlarged by more than 5 times (i.e., from 4.5 to 30 mT) compared with the control sample. On the other hand, H_c does not change monotonically with d_1. Instead, when the top surface is 6 QL away from the bottom layer, we observe the minimum H_c of only 2.5 mT. Similarly, if we extract the Curie temperature T_c from the $H_c - T$ curves in Figure 2d−f, we have the highest T_c (10.9 K) for Sample **B**, compared with 7.4 and 6.9 K in Samples **A** and **C**, respectively. Here, since the identical bottom Cr-doped TI layers of the three samples contribute the same "bulk" magnetization, the change of both H_c and T_c among them hence can only be associated with the separation between the top surface and the bulk Cr ions. Therefore, both the unique d_1-dependent magnetization behavior and the enhancement of T_c in Sample **B** may provide us with the direct evidence about the presence of the surface-related ferromagnetism in modulation-doped TI thin films.

To further investigate the intrinsic mechanism of the surface-related magnetic response, we fabricate micrometer-size top-gated Hall bar devices to carry out the electric-field-controlled magneto-transport measurements on the modulation-doped TI heterostructures. Because of the low defects achieved in the growth, the electric field provided by top gate (± 12 V) can effectively tune the E_F across the Dirac point, and therefore change the carrier type in all the bilayer samples (Supporting Information S7). Figure 3a−d presents the top-gate-dependent anomalous Hall effects (AHE) in four $(Bi_{0.5}Sb_{0.5})_2Te_3$/$Cr_{0.16}(Bi_{0.54}Sb_{0.38})_2Te_3$ bilayer films with different top TI layer thicknesses, $d_1 = 2$ QL, 3 QL, 4 QL, and 6 QL, respectively. When d_1 is below 6 QL, R_{xy} loops in Figure 3a−c all exhibit a typical hole-mediated RKKY coupling feature in the p-type region, where the magnetic hysteresis window gradually shrinks as the holes are depleted by the increase of V_g. Similar to the MOKE data in Figure 2, it is also interesting to observe that the AHE signal (in terms of H_c) is most enhanced when $d_1 = 3$ QL. On the contrary, when the top layer thickness is further

increased to $d_1 = 6$ QL, the electric-field has no effect on the AHE signal at all, and H_c remains at 20 mT for all applied V_g, as shown in Figure 3d. Apart from the d_1-dependent AHE measurements, information regarding novel magneto-electric effects is also obtained from the magneto-resistance (MR) results. Figure 3e−hs provide three-dimensional normalized MR maps as a function of applied V_g for the same samples as given in Figure 3a−d. Conventional butterfly-shaped double-split MR peaks are observed, and the peak positions that deviate from $B = 0$ T directly indicate the remnant field generated by the ferromagnetic moments.[36] In agreement with the AHE observations, the tunability of the MR peak position by external electric-field depends on the top layer thickness d_1, and the separation of the split peaks reaches the maximum value (i.e., 140 mT in Figure 3f) in the "optimized" $d_1 = 3$ QL sample. More importantly, as long as $d_1 < 6$ QL, the MR curves always display a weak localization (WL) effect, where the conduction of the surface carriers is affected by the underneath Cr impurities and the corresponding destructive quantum interference in turn gives rise to the negative MR cusps at low magnetic field.[28,44] On the contrary, the development of the negative weak antilocalization (WAL) cusp around zero field becomes clear only when d_1 increases to 6 QL (Figure 3h). Together with the gate-insensitive hysteresis behaviors, the WL-to-WAL crossover may imply that the reappearance of massless Dirac-fermions on the top surface given that the separation d_1 is large enough to prevent strong magnetic coupling from the underlying magnetic impurities (see details in Supporting Information Figure S8).[44−46]

In order to quantitatively examine the d_1-dependent magneto-electric responses, we subsequently compare the $H_c−V_g$ results of the TI/Cr-doped TI bilayer samples with their top layer thicknesses varying from 0 QL to 5 QL in Figure 4a. Here, the unveiled monotonically decreasing relation of $H_c−V_g$ in the p-type region (i.e., $−12$ V $< V_g < 5$ V) possibly suggests that one of the prevailing magnetic mechanisms in the $Cr_{0.16}(Bi_{0.54}Sb_{0.38})_2Te_3$ based bilayer films (with $d_1 < 6$ QL) is

introduced by the hole-mediated RKKY interaction. As we elaborate in Supporting Information S9, similar to bulk itinerant carriers, the surface holes are also much more favored for mediating the p-d exchange coupling in the Cr-doped $(Bi_xSb_{1-x})_2Te_3$ TIs compared with surface electrons, given the fact that the density-of-states (DOS) of the 3d Cr ion mostly distributes below the Dirac point in the bulk band gap.[12] In the meanwhile, due to the effective Fermi level tuning, the coercivity fields H_c are found to achieve over 100% modulation via gate-voltage control in all samples with d_1 varying from 0 QL to 4 QL; the most pronounced change is obtained in the 3 QL TI/6 QL Cr-doped TI sample, as illustrated in Figure 4b. Specifically, H_c decreases steadily from 135 mT down to 65 mT with the depletion of the holes, and the corresponding electric-field-controlled coercivity field change ($\Delta H_c = 70$ mT) is three times larger than the uniformly doped control sample ($\Delta H_c = 20$ mT). It is important to point out that the Debye length of our grown modulation-doped TI bilayer films is estimated to be less than 3 nm at 1.9 K when the samples are biased in the inversion/accumulation regions (i.e., n/p-type).[47,48] On the basis of our device geometry, it implies that the applied top-gate voltage is only able to tune the Fermi level of the top surface states. Accordingly, we may conclude that the magneto-electric responses among the modulation-doped TI heterostructures in the p-type regions are predominantly due to the variations of the surface-related ferromagnetism, and the pronounced enhancement of ΔH_c may reflect the optimization of the magnetic RKKY coupling between neighboring Cr ions through top surface states. Furthermore, it should be also noted that since the screening effect limits the effect of the external electric-field beyond the top surface region when the surface Fermi level is tuned away from the Dirac point, the bulk magnetizations (i.e., van Vleck mechanism or bulk-carrier-mediated RKKY interaction) hence are almost irrelevant to the top-gate bias. Under the circumstance where the top-surface-related magnetic order is minimized, both the carrier-independent AHE signals observed in the $d_1 = 6$ QL sample (Figure 3d) and the nonzero magnetization remaining in the n-type regions for $d_1 < 6$ QL samples ($V_g > 5$ V in Figure 4a) can possibly be attributed to the bulk ferromagnetism (i.e., not mediated by the top-surface-related effects).

To understand the optimization behavior of the surface-mediated magneto-electric effect in the 3QL $(Bi_{0.5}Sb_{0.5})_2Te_3$/6 QL $Cr_{0.16}(Bi_{0.54}Sb_{0.38})_2Te_3$ bilayer device, we consider the surface-mediated RKKY interaction in our system[34,49−51]

$$\hat{H}_{ex}^{RKKY} = \sum_{i,j} \Phi_{i,j}(|r - r'|)S_{1i}(r)S_{2j}(r') \tag{1}$$

where $\Phi_{ij}(R)$ is the coupling strength between two neighboring magnetic impurities, and $S_i(r)$ is the local magnetic spin. It is known that the density of surface carriers follows the $n_s(d) \propto e^{-2d/D_0}$ distribution relation and D_0 characterizes the penetration depth of the surface states with a typical value of 2−3 QLs.[52,53] At the same time, because the RKKY coupling is a second-order-perturbation interaction, its exchange strength is thus inversely proportional to the energy difference between the ground and the excited states (i.e., the surface band gap opening Δ_0).[51] Accordingly, the overall exchange strength follows

$$\langle \Phi(d_1) \rangle = \Phi_0 e^{-2d_1/D_0} \frac{\Delta_0}{\Delta_1 e^{-d_1/D_1} + \Delta_{dipole}} \tag{2}$$

where Φ_0 is the RKKY interaction strength in the uniformly Cr-doped TI film and $\Delta_0 = \Delta_1 + \Delta_{dipole}$ is the total surface gap opening which takes into account both the direct magnetic exchange field (Δ_1) and the long-range magnetic dipolar field (Δ_{dipole}) from the doped Cr ions. In our TI/Cr-doped TI bilayer systems, as the mediating carriers itinerate within the top surface states, the resulting exchange coupling will thus decay exponentially with the separation distance (d_1). In the dilute magnetic doping case, the exchange coupling length d_1 only depends on the Cr dopant itself (i.e., the dopant's type and its outer-shell orbital manifold),[13,54] and Δ_{dipole} can be regarded as a constant (i.e., it does not change with d_1) under the mean-field approximation.[55] From eq 2 and the schematic representations in Figure 3i−l, it is observed that by increasing d_1, the top topological surface state experiences a smaller perpendicular magnetic exchange field, which results in the decrease of the surface gap opening. On the other hand, since n_s also exponentially decays from the top surface into the bulk, it therefore lowers the participation of surface carriers in the RKKY mediation process. Consequently, it can be expected that these two competing mechanisms will result in a counter-balanced situation where the overall surface-mediated RKKY interaction $\langle \Phi(d_1) \rangle$ becomes the highest at the critical top layer thickness $d_1 = d_c$. Besides, it is also reasonable to infer that once the top surface detaches from the bottom magnetic layer (i.e., $d_1 > d_{max}$), $\langle \Phi(d_1) \rangle$ would vanish due to the infinitesimally small value of e^{-2d_{max}/D_0} and therefore, lead to a vanishing surface-related ferromagnetic order. Based on the above scenario, we are able to estimate the d_1-dependent exchange strength, as given in Supporting Information Figure S10, and it is consistent with the experimental observations as shown in Figure 2−4.

In addition to the above realization of intrinsic magnetism, understanding the underlying magnetic phase transition and the Curie temperature (T_c) is equally important. Figure 4c shows a three-dimensional map of T_c in which T_c is estimated from the evolution of the coercivity field H_c under different temperatures and the gate voltages in the 4 QL TI/6 QL Cr-doped TI bilayer sample. Since T_c is the measure of the transition from the ferromagnetic to paramagnetic state, the magnetic hysteresis window is therefore expected to be closed (i.e., H_c becomes zero) when the temperature is approaching T_c. As an example, the temperature evolution of H_c under a fixed electric field of $V_g = -12$ V is given in Figure 4d, and the Curie temperature is extracted to be $T_c = 7.3 \pm 0.2$ K. Besides, Figure 4e displays the gate-dependent T_c and the corresponding carrier density n_{2D}−V_g curves. As V_g increases progressively from negative to positive, T_c reduces, and the calculated Hall density systematically changes from p-type to n-type, which also suggests the presence of the hole-mediated RKKY mechanism.[36]

The realization of surface-related ferromagnetism in Cr-doped $(Bi_{1-x}Sb_x)_2Te_3$ films may provide a new platform for the further discovery of exotic TRS-breaking topological physics. Additionally, the direct engineering of the surface-mediated RKKY interaction in modulation-doped TI bilayer systems may further facilitate the exploration of new applications in TI-based heterostructures and supperlattices.

■ ASSOCIATED CONTENT

Ⓢ Supporting Information

In-situ monitor of modulation-doped topological insulators growth. Elemental mappings of Cr-$(Bi_xSb_{1-x})_2Te_3$ thin films by EDX. Surface gap opening in Cr-doped TIs by ARPES.

Impedance-match for 6 QL $(Bi_xSb_{1-x})_2Te_3$ and Cr-$(Bi_xSb_{1-x})_2Te_3$ thin films. Quantum interference in modulation-doped TI/Cr-doped TI structures. Ambipolar effects in modulation-doped TI/Cr-doped TI structures. Surface-mediated RKKY interaction model in Cr-doped 3D TIs. Physical model to explain the manipulation of surface-related magnetoelectric effects in modulation-doped TI/Cr-doped TI structures. Polar MOKE setup. Calculation of the penetration depth. This material is available free of charge via the Internet at http://pubs.acs.org.

■ AUTHOR INFORMATION

Corresponding Authors
*E-mail: (K.W.) wang@ee.ucla.edu.
*E-mail: (L. H.) heliang@ee.ucla.edu.
Author Contributions
∥X.K., L.H., and M.L. contributed equally to this work.
Notes
The authors declare no competing financial interest.

■ ACKNOWLEDGMENTS

■ REFERENCES

(1) Kane, C. L.; Mele, E. J. *Phys. Rev. Lett.* **2005**, *95*, 146802.
(2) Kane, C. L.; Mele, E. J. *Phys. Rev. Lett.* **2005**, *95*, 226801.
(3) Bernevig, B. A.; Hughes, T. L.; Zhang, S. C. *Science* **2006**, *314* (5806), 1757−1761.
(4) Moore, J. E.; Balents, L. *Phys. Rev. B* **2007**, *75* (12), 121306.
(5) Fu, L.; Kane, C. L.; Mele, E. J. *Phys. Rev. Lett.* **2007**, *98*, 106803.
(6) Jiang, Y. P.; Wang, Y. L.; Chen, M.; Li, Z.; Song, C. L.; He, K.; Wang, L. L.; Chen, X.; Ma, X. C.; Xue, Q. K. *Phys. Rev. Lett.* **2012**, *108*, 016401.
(7) Xu, S. Y.; Xia, Y.; Wray, L. A.; Jia, S.; Meier, F.; Dil, J. H.; Osterwalder, J.; Slomski, B.; Bansil, A.; Lin, H.; Cava, R. J.; Hasan, M. Z. *Science* **2011**, *332* (6029), 560−564.
(8) Konig, M.; Wiedmann, S.; Brune, C.; Roth, A.; Buhmann, H.; Molenkamp, L. W.; Qi, X. L.; Zhang, S. C. *Science* **2007**, *318* (5851), 766−770.
(9) Hsieh, D.; Qian, D.; Wray, L.; Xia, Y.; Hor, Y. S.; Cava, R. J.; Hasan, M. Z. *Nature* **2008**, *452* (7190), 970−U5.
(10) Qi, X. L.; Zhang, S. C. *Phys. Today* **2010**, *63* (1), 33−38.
(11) Zhang, Y.; He, K.; Chang, C. Z.; Song, C. L.; Wang, L. L.; Chen, X.; Jia, J. F.; Fang, Z.; Dai, X.; Shan, W. Y.; Shen, S. Q.; Niu, Q.; Qi, X. L.; Zhang, S. C.; Ma, X. C.; Xue, Q. K. *Nat. Phys.* **2010**, *6* (8), 584−588.
(12) Zhang, J. M.; Zhu, W. G.; Zhang, Y.; Xiao, D.; Yao, Y. G. *Phys. Rev. Lett.* **2012**, *109*, 266405.
(13) Liu, Q.; Liu, C. X.; Xu, C. K.; Qi, X. L.; Zhang, S. C. *Phys. Rev. Lett.* **2009**, *102*, 156603.
(14) Liu, C. X.; Qi, X. L.; Dai, X.; Fang, Z.; Zhang, S. C. *Phys. Rev. Lett.* **2008**, *101*, 146802.
(15) Yu, R.; Zhang, W.; Zhang, H. J.; Zhang, S. C.; Dai, X.; Fang, Z. *Science* **2010**, *329* (5987), 61−64.
(16) Jiang, H.; Qiao, Z. H.; Liu, H. W.; Niu, Q. *Phys. Rev. B* **2012**, *85*, 045445.
(17) Qi, X. L. *Phys. Rev. Lett.* **2011**, *107*, 120501.
(18) Chang, C. Z.; Zhang, J.; Feng, X.; Shen, J.; Zhang, Z.; Guo, M.; Li, K.; Ou, Y.; Wei, P.; Wang, L. L.; Ji, Z. Q.; Feng, Y.; Ji, S.; Chen, X.; Jia, J.; Dai, X.; Fang, Z.; Zhang, S. C.; He, K.; Wang, Y.; Lu, L.; Ma, X. C.; Xue, Q. K. *Science* **2013**, *340* (167), 4.
(19) Qi, X. L.; Hughes, T. L.; Zhang, S. C. *Phys. Rev. B* **2008**, *78*, 195424.
(20) Tserkovnyak, Y.; Loss, D. *Phys. Rev. Lett.* **2012**, *108*, 187201.
(21) Hasan, M. Z.; Kane, C. L. *Rev. Mod. Phys.* **2010**, *82* (4), 3045−3067.
(22) Zhang, Y. Y.; Wang, X. R.; Xie, X. C. *J. Phys.: Condens. Matter* **2012**, *24*, 1.
(23) Li, R. D.; Wang, J.; Qi, X. L.; Zhang, S. C. *Nat. Phys.* **2010**, *6* (4), 284−288.
(24) Moore, J. E. *Nature* **2010**, *464* (7286), 194−198.
(25) Moore, J. *Nat. Phys.* **2009**, *5* (6), 378−380.
(26) Fu, L.; Kane, C. L. *Phys. Rev. Lett.* **2009**, *102*, 216403.
(27) Akhmerov, A. R.; Nilsson, J.; Beenakker, C. W. J. *Phys. Rev. Lett.* **2009**, *102*, 216404.
(28) Liu, M. H.; Zhang, J. S.; Chang, C. Z.; Zhang, Z. C.; Feng, X.; Li, K.; He, K.; Wang, L. L.; Chen, X.; Dai, X.; Fang, Z.; Xue, Q. K.; Ma, X. C.; Wang, Y. Y. *Phys. Rev. Lett.* **2012**, *108*, 036805.
(29) Chen, Y. L.; Chu, J. H.; Analytis, J. G.; Liu, Z. K.; Igarashi, K.; Kuo, H. H.; Qi, X. L.; Mo, S. K.; Moore, R. G.; Lu, D. H.; Hashimoto, M.; Sasagawa, T.; Zhang, S. C.; Fisher, I. R.; Hussain, Z.; Shen, Z. X. *Science* **2010**, *329* (5992), 659−662.
(30) Xu, S. Y.; Neupane, M.; Liu, C.; Zhang, D. M.; Richardella, A.; Wray, L.; Alidoust, N.; Leandersson, M.; Balasubramanian, T.; Barriga, J.; Rader, O.; Landolt, G.; Slomski, B.; Dil, J. H.; Osterwalder, J.; Chang, T. R.; Jeng, H. T.; Lin, H.; Bansil, A.; Samarth, N.; Hasan, A. *Nat. Phys.* **2012**, *8*, 616−622.
(31) Wray, L. A.; Xu, S. Y.; Xia, Y. Q.; Hsieh, D.; Fedorov, A. V.; Hor, Y. S.; Cava, R. J.; Bansil, A.; Lin, H.; Hasan, M. Z. *Nat. Phys.* **2011**, *7* (1), 32−37.
(32) Abanin, D. A.; Pesin, D. A. *Phys. Rev. Lett.* **2011**, *106*, 136802.
(33) Kou, X. F.; Jiang, W. J.; Lang, M. R.; Xiu, F. X.; He, L.; Wang, Y.; Wang, Y.; Yu, X. X.; Fedorov, A. V.; Zhang, P.; Wang, K. L. *J. Appl. Phys.* **2012**, *112*, 063912.
(34) Zhu, J. J.; Yao, D. X.; Zhang, S. C.; Chang, K. *Phys. Rev. Lett.* **2011**, *106*, 097201.
(35) Chang, C. Z.; Zhang, J. S.; Liu, M. H.; Zhang, Z. C.; Feng, X.; Li, K.; Wang, L. L.; Chen, X.; Dai, X.; Fang, Z.; Qi, X. L.; Zhang, S. C.; Wang, Y. Y.; He, K.; Ma, X. C.; Xue, Q. K. *Adv. Mater.* **2013**, *25* (7), 1065−1070.
(36) Checkelsky, J. G.; Ye, J. T.; Onose, Y.; Iwasa, Y.; Tokura, Y. *Nat. Phys.* **2012**, *8*, 729−733.
(37) Judaprawira, S.; Wang, W. I.; Chao, P. C.; Wood, C. E. C.; Woodard, D. W.; Eastman, L. F. *Electron Device Lett.* **1981**, *2* (1), 14−15.
(38) Wu, S. L.; Chang, S. J. *Solid-State Electron.* **1999**, *43* (7), 1313−1316.
(39) Yoon, S. F.; Miao, Y. B.; Radhakrishnan, K.; Duan, H. L. *Superlattices Microstruct.* **1996**, *19* (3), 159−167.
(40) Zhang, W.; Yu, R.; Zhang, H.-J.; Dai, X.; Fang, Z. *New J. Phys.* **2010**, *12*, 065013.
(41) Hong, S. S.; Cha, J. J.; Kong, D. S.; Cui, Y. *Nat. Commun.* **2012**, *3*, 757.
(42) Arakane, T.; Sato, T.; Souma, S.; Kosaka, K.; Nakayama, K.; Komatsu, M.; Takahashi, T.; Ren, Z.; Segawa, K.; Ando, Y. *Nat. Commun.* **2012**, *3*, 636.

(43) Lang, M. R.; He, L.; Kou, X. F.; Upadhyaya, P.; Fan, Y. B.; Chu, H.; Jiang, Y.; Bardarson, J. H.; Jiang, W. J.; Choi, E. S.; Wang, Y.; Yeh, N. C.; Moore, J.; Wang, K. L. *Nano Lett.* **2013**, *13* (1), 48−53.

(44) Lu, H. Z.; Shi, J. R.; Shen, S. Q. *Phys. Rev. Lett.* **2011**, *107*, 076801.

(45) Nestoklon, M. O.; Averkiev, N. S.; Tarasenko, S. A. *Solid State Commun.* **2011**, *151* (21), 1550−1553.

(46) He, H. T.; Wang, G.; Zhang, T.; Sou, I. K.; Wong, G. K. L.; Wang, J. N.; Lu, H. Z.; Shen, S. Q.; Zhang, F. C. *Phys. Rev. Lett.* **2011**, *106*, 166805 .

(47) Sze, S. M.; Ng, K. K. *Physics of semiconductor devices*; John Wiley and Sons: New Jersey, 2006.

(48) Sacepe, B.; Oostinga, J. B.; Li, J.; Ubaldini, A.; Couto, N. J. G.; Giannini, E.; Morpurgo, A. F. *Nat. Commun.* **2011**, *2*, 575.

(49) Ruderman, M. A.; Kittel, C. *Phys. Rev.* **1954**, *96* (1), 99−102.

(50) Yosida, K. *Phys. Rev.* **1957**, *106* (5), 893−898.

(51) Rosenberg, G.; Franz, M. *Phys. Rev. B* **2012**, *85* (19), 195119.

(52) Li, Y.-Y.; Wang, G.; Zhu, X.-G.; Liu, M.-H.; Ye, C.; Chen, X.; Wang, Y.-Y.; He, K.; Wang, L.-L.; Ma, X.-C.; Zhang, H.-J.; Dai, X.; Fang, Z.; Xie, X.-C.; Liu, Y.; Qi, X.-L.; Jia, J.-F.; Zhang, S.-C.; Xue, Q.-K. *Adv. Mater.* **2010**, *22* (36), 4002−4007.

(53) Zhang, W.; Yu, R.; Zhang, H. J.; Dai, X.; Fang, Z. *New J. Phys.* **2010**, *12*, 065013.

(54) Coey, J. M. D., *Magnetism and Magnetic Materials*; Cambridge: New York, 2010.

(55) Loudon, R. *Phys. Rev.* **1960**, *119* (3), 919−921.